Field-Free All-Optical Switching and Electrical Readout of Tb/Co-Based Magnetic Tunnel Junctions

D. Salomoni,[1,*] Y. Peng,[2] L. Farcis,[1] S. Auffret,[1] M. Hehn,[2] G. Malinowski,[2] S. Mangin,[2] B. Dieny,[1]
L.D. Buda-Prejbeanu,[1] R.C. Sousa,[1] and I.L. Prejbeanu[1,†]

[1]*Université Grenoble Alpes, Alternative Energies and Atomic Energy Commission (CEA), CNRS, Institut
Polytechnique de Grenoble, Spintronique et Technologie des Composants (SPINTEC), Grenoble 38000, France*
[2]*Institut Jean Lamour, UMR CNRS 7198, Université de Lorraine, Nancy 54011, France*

The switching of a magnetic tunnel junction (MTJ) using femtosecond laser pulses enables a possible path for nonvolatile, ultrafast, and low-dissipative memories. In this work, we demonstrate successful field-free 50-fs single-laser-pulse-driven magnetization reversal of a [Tb/Co]-based storage layer in a perpendicular MTJ with a estimated absorbed energy of 68.6 fJ/bit. The nanofabricated MTJ devices have an optimized bottom reference electrode and show tunnel-magnetoresistance-ratio (TMR) values up to 74% after patterning down to sub-100-nm lateral dimensions. Experiments on continuous films reveal peculiar reversal patterns of concentric rings with opposite magnetic directions, above a certain threshold fluence. These rings have been correlated with the patterned-device switching probability as a function of the applied laser fluence. Moreover, the magnetization reversal is independent of the duration of the laser pulse. According to our macrospin model, the underlying magnetization-reversal mechanism can be attributed to an in-plane reorientation of the magnetization due to a fast reduction of the out-of-plane uniaxial anisotropy and a magnetization precession around the local effective-anisotropy axis. These aspects are of great interest both for the physical understanding of the switching phenomenon and their consequences for all-optical-switching memory devices, since they allow for a large fluence operation window with high resilience to pulse-length variability.

I. INTRODUCTION

Conventional computer memories have evolved into a many-level hierarchy where the operation speed, storage density, and cost define a trade-off leading to the implementation of different memory technologies. As the physical limits of complementary metal oxide semiconductor (CMOS) memories are reached, the possibility of replacing volatile memory with fast nonvolatile alternatives has been a compelling argument for magnetoresistive random access memory (MRAM) [1–3]. Perpendicular spin-transfer-torque (STT) MRAM, due to advantages such as reliable switching, low energy consumption, and easy integration with CMOS technology [1], is the most widely foundry-adopted spintronics-based memory [4–6]. High-performance STT magnetic tunnel junction (MTJ) cells are among the first MRAMs to have recently been commercialized as embedded flash memory and last-level cache replacements. The (Fe-Co-B)–MgO–(Fe-Co-B) system has become the basis of most MTJ designs, due

*david.salomoni@cea.fr
†ioan-lucian.prejbeanu@cea.fr

to its high tunnel-magnetoresistance-ratio (TMR) effect [7,8], improved readability, and the scaling of interfacial perpendicular-magnetic-anisotropy- (PMA) based [9] devices. Moreover, in STT cells, the reading and writing paths are shared, enabling a compact design [10,11]; however, fast switching in the precessional regime requires switching voltages close to the barrier breakdown voltage.

The alternative spin-orbit torque (SOT) technology is more suitable for high-speed and low-error-rate operation [12,13]. SOT three-terminal devices with separate reading and writing paths enable better endurance combined with fast switching, creating a potential replacement for static random access memories (SRAMs) [14]. The main drawback of SOT is the larger bit-cell area and although switching pulses as short as 100 ps are possible, the application of a field is generally required to obtain deterministic switching, which complicates the cell design.

The all-optical-switching (AOS) technology envisions further acceleration of the magnetization-reversal process by enabling writing of the cells on femtosecond time scales. Single-pulse all-optical helicity-independent switching (AO HIS) is a phenomenon by which the magnetization of a nanostructure can be reversed by a single

femtosecond laser pulse. The method is ultrafast and does not require use of any applied field. Since its discovery in Fe-Co-B ferrimagnetic systems [15], single-pulse AO HIS had been limited to Gd-based alloys or Gd/FM bilayers, where FM is a ferromagnetic layer [16,17]. Only recently, a few other material systems have shown switching driven by ultrashort laser pulses: MnRuGa ferrimagnetic Heusler alloys [18], Tb/Co multilayers [19–21], and Tb/Fe and the $Tb_{32}Co_{68}/Co/Tb_{32}Co_{68}$ trilayer [22]. An encouraging alternative spin-valve mechanism has been recently explored in Ref. [23], where angular momentum is brought from one layer to the other, allowing rare-earth free switching. As demonstrated in this paper, the AO-HIS mechanism for Tb-based heterostructures is very different than the one observed for Gd-based materials.

The use of AOS as a write mechanism in MRAM is expected to enable writing at speeds 2 orders of magnitude faster than electrical alternatives with an energy as low as 16 fJ/bit [3], while maintaining nonvolatility [3,18]. This not only increases speed and reduces power consumption but also allows for more compact two-terminal design of STT devices, with no compromise in endurance.

The first successful AOS operation of a micron-sized *p*-MTJ cell was demonstrated by Chen *et al.* [24], using a Fe-Co-B–alloy storage layer, leading to a small TMR ratio of 0.6%. This was later improved by Wang *et al.* [25], who reported switching of Co/Gd bilayer tunnel junctions with cell sizes down to 3 μm lateral size and a TMR ratio of 34.7%. The increase in the TMR was possible due to a clever design demonstrated by Avilés-Félix *et al.* [19,20,26], where to enable AOS in an MTJ, the optically switchable material is coupled magnetically to the Fe-Co-B interface of the storage layer. The initial reports of a storage layer based on a $[Tb/Co]_N$ multilayer coupled to a Fe-Co-B showed the possibility of adjusting the Co/Tb composition in order to control the effective perpendicular anisotropy of MTJs [19,20]. The perpendicular anisotropy could be maintained without degradation even after annealing at 250 °C to obtain 38% TMR after patterning. Thin-film experiments of the same storage-layer stacks have confirmed AO HIS of the magnetization with both 60-fs and 5-ps laser pulses for incident fluences down to 3.5 mJ/cm². However, reliable and field-free AOS demonstrations on patterned devices and a clear understanding of the switching mechanism of this system are missing so far.

In this work, we have developed MTJ devices comprising a $[Tb/Co]_5$-based top storage layer with diameters from 300 nm down to 80 nm, exhibiting TMR values up to 74%. We demonstrate field-free helicity-independent all-optical toggle switching driven by 50-fs single light pulses on a [Tb/Co]-based *p*-MTJ patterned to sub-100-nm lateral dimensions. The comparison of the patterned-device properties to those of continuous film shows that high anisotropy of the Tb/Co-based electrode is maintained

after patterning. The integration of a stable reference layer, with a low offset field, does not degrade the properties of the AOS stack. Furthermore, the AOS behavior seen at film level correlates with the patterned-device switching probability, despite the evident changes in the magneto-static interaction. The underlying reversal mechanism that takes place in these systems is analyzed in the framework of a macrospin model accounting for the temperature dependence of the anisotropy.

II. RESULTS AND DISCUSSION

Our samples depicted in Fig. 1(a) have a bottom synthetic antiferromagnetically (SAF) coupled-reference-layer-based [Co/Pt] multilayer, like the one used in conventional STT-MRAM cells. The complete magnetic stack deposited by dc magnetron sputtering is Ta(3 nm)/ Pt(25 nm)/[Co(0.5 nm)/Pt(0.25 nm)]×5/Co(0.5 nm)/Ru
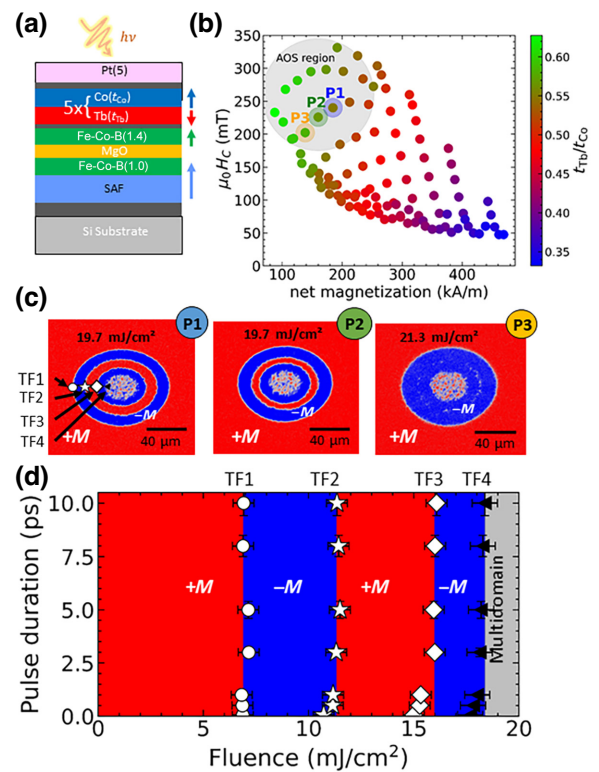

FIG. 1. (a) A schematic of the AOS-MTJ stack with a bottom-pinned and [Tb/Co]-based storage layer. (b) The MOKE-magnetometer-measured coercive field versus the net magnetization, $M_{rmS,Co} = 760$ kA/m, $M_{rmS,Tb} = 1350$ kA/m [27,28]. (c) Background-subtracted MOKE images after single 50-fs laser pulses of different fluences and for the following positions: P1—t_{Co}, 1.37 nm; t_{Tb}, 0.76 nm; P2—t_{Co}, 1.41 nm; t_{Tb}, 0.80 nm; P3—t_{Co}, 1.45 nm; t_{Tb}, 0.86 nm. (d) An experimental state diagram of the pulse duration versus the fluence of the magnetization reversal. Threshold (ring) boundaries: TF1, outer-border red to blue; TF2, blue to red border; TF3, second red to blue border; TF4, center demagnetized multidomain.

(0.9 nm)/[Co(0.5 nm)/Pt(0.25 nm)]×2/Co(0.5 nm)/W (0.3 nm)/(Fe-Co-B)(1 nm)/MgO(t_{Mg})/(Fe-Co-B)(1.4 nm)/ W(0.2 nm)/[Tb(t_{Tb})/Co(t_{Co})]×5/W(2 nm)/Pt(5 nm). Samples were deposited using Ar pressure of 2×10^{-3} mbar and a base pressure of 10^{-8} mbar and annealed at 250 °C. The samples were deposited using a double-wedge thicknesses for Tb and either MgO or Co to allow for the investigation of device properties as a function of the layer thickness, as in Ref. [19].

The AO-HIS properties of our multilayered samples before nanopatterning were systematically analyzed by magneto-optical Kerr-effect microscopy (MOKE). The pump laser beam used in the AOS measurement was generated by a Ti:sapphire femtosecond-laser source with a wavelength of 800 nm and a repetition rate of 5 kHz. The Gaussian-beam diameter of 100 µm was determined by directly observing the beam at the focal plane of the microscope lens and was later confirmed using the reversed domain size as a function of the pulse energy. The source for the background-subtracted MOKE images, depicted in Figs. 1(c) and 2(b), was a light-emitting diode (LED), operating at a wavelength of 628 nm. The measurements were carried out without a requirement for synchronization, as they were conducted under static conditions. The methodology consisted of applying individual laser shots followed by a sample measurement after each pulse. Depending on the substrate material, either a transmission or reflection configuration was employed: transmission for glass substrates and reflection for silicon substrates (for further details, see Ref. [22]). Regardless of the configuration, the system shows AOS close to the magnetization compensation region at room temperature and in the Co-rich region where the Co magnetization is dominant, no significant differences are found for the two types of substrates. Similar to previous reported [Tb/Co] multilayers [20] with five bilayer repetitions annealed at 250 °C, the Tb thickness range is from 0.6 to 0.9 nm and, respectively, 1.2 to 1.5 nm for Co. Figure 1(b) shows the coercive field versus the net magnetization for the Tb/Co thickness ratio, with the highlighted region showing where AOS is occurring (gray area). The net magnetization was determined based on the thickness of the deposited Tb and Co layers, using M_{rmS} values from Refs. [27,28]. We used a MOKE magnetometer for the measurements, enabling us to pinpoint the magnetization compensation point and address possible fluctuations in the deposition rate and disparities from established M_S values in the literature sources. As one can see, to have AOS, the system needs to be close to the compensation point, where M_S is relatively low and the anisotropy, which is proportional to the coercive field, is high. In this AOS thickness region, a strong reduction in the anisotropy and an increase in the net magnetization with the temperature have been shown in Refs. [21,22].

After each single laser pulse, a complete full-signal amplitude toggle reversal of the storage layer occurs. This behavior is reproducible for the storage-layer stack up to 150 000 consecutive pulses, suggesting that the toggle switching has a large endurance and repeatability for the above thickness ranges.

For fluences higher than 11 mJ/cm², the reversed domains exhibit concentric rings with opposite magnetic directions [as seen in Figs. 1(c) and 2(b)]. It is noteworthy that similar behavior has also been observed for samples with only [Tb/Co] multilayers, excluding any contribution from the SAF reference layer to the magnetization reversal, except for its impact as a heat-sink structure increasing the fluence threshold of the different regions [22]. From the outside inward, four fluence thresholds (TF1-TF4), for reversal or nonreversal, were identified, taking into account the Gaussian profile of the laser spot. Based on the MOKE observation upon varying the laser pulse duration, it was possible to draw a complete state diagram of the pulse duration versus the fluence, as reported in Fig. 1(d). The type of reversal, either concentric rings or single domain, is dependent on the respective multilayer thicknesses. As shown in Fig. 1(c) for positions P1, P2, and P3, the threshold fluences TF2 and TF3 defining the presence of the second ring, having the same magnetization as the initial state (red contrast), are brought closer with increasing Tb and Co thicknesses, merging together for Tb(0.86 nm)/Co(1.45 nm) at P3, to form a single reversed domain. This effect can be assigned to an increase in the Gilbert damping due to the increased Tb content [29,30]. As reported in Ref. [22] and contrary to Gd-based materials, the fluence required to reverse and stabilize a given number of rings has little or no dependence on the laser pulse duration. Single-pulse reversals were obtained for pulse durations from 50 fs up to 12 ps, the maximum pulse duration available on the laser setup.

We have recently studied the possible origin of these peculiar AOS properties pointing toward an in-plane magnetization reorientation with a precessional switching mechanism. The reported state diagrams observed for Tb/Fe and for the $Tb_{32}Co_{68}$/Co/$Tb_{32}Co_{68}$ trilayer [22] share the same similarities as those of the [Tb/Co] multilayers, proving that a similar magnetization-reversal process takes place in these Tb-based multilayer systems.

The independence of pulse duration suggests that the reversal mechanism proceeds for a longer time than the laser pulse itself and is slower than the one observed in Gd-based samples [16]. Considering a two-temperature model, at the short time scale up to a few picoseconds, the behavior of the electron temperature, T_e, is highly dependent on the laser pulse duration. Within a few picoseconds, T_e relaxes to the phonon temperature T_p and, from there, on, the time evolution of the two becomes indistinguishable. For longer times, of the order of tens to hundreds of picoseconds, the temperatures reached are only due to the laser fluence and the cooling of the system to the thermal bath. Based on the experimental results, we understand
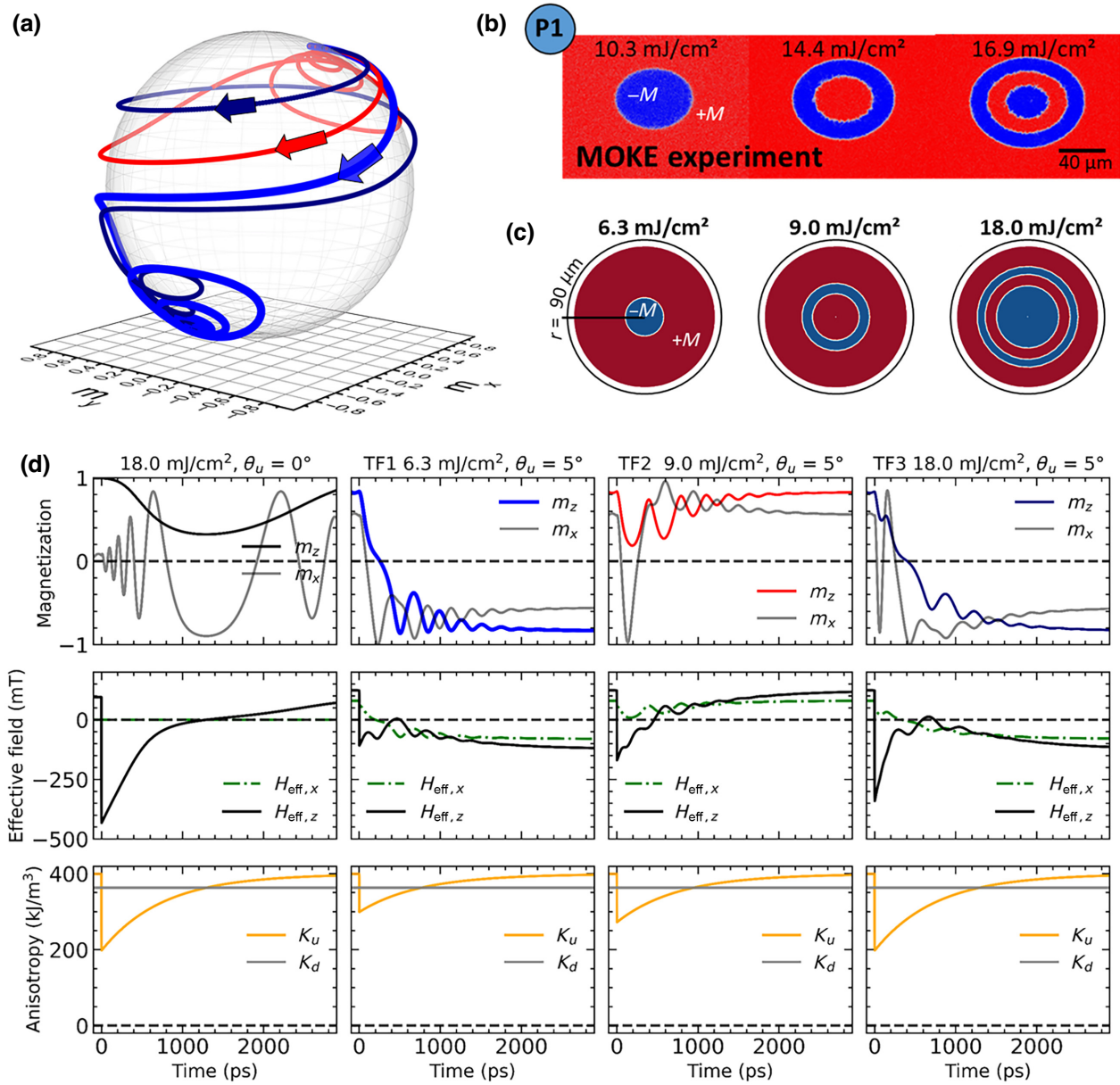
FIG. 2. (a) A three-dimensional view of the magnetization dynamics as predicted by the macrospin model. (b) For position P1 [Fig. 1(b)], experimental background-subtracted MOKE images, laser: 50 fs and 10.3 mJ/cm^2, 14.4 mJ/cm^2, and 16.9 mJ/cm^2. (c) The expected magnetization pattern after 100 fs for a single Gaussian-shaped laser pulse with fully independent spins. The simulations in (a) and (c) were performed for $\theta_u = 5°$, $M_s = 760$ kA/m, $K_{u,300K} = 1.1 \times (\mu_0 M_s^2/2)$, and Gilbert damping $\alpha = 0.1$. (d) $m_z, m_z, H_{eff,x}, H_{eff,z}$, and K_u time traces for $\theta_u = 5°$ fluences 6.3 mJ/cm^2, 9.0 mJ/cm^2, 18.0 mJ/cm^2, and $\theta_u = 0°$ fluences 18.0 mJ/cm^2.

that the key dynamics for the reversal occur during the longer time phase. This interpretation is based on the fact that superdiffusive spin currents [31], hot electrons, and ultrafast demagnetization [32] are effects that are highly dependent on the pulse duration. This is contrary to our experimental observations, where the final reversed state is essentially independent of the laser pulse length up 12 ps and probably beyond. The initial fast response phase certainly plays a role at the beginning of the reversal, and

may be more important for femtosecond pulses, but does not determine the end state.

Hence, we have developed a phenomenological macro-spin model based on the Landau-Lifshitz-Gilbert equation coupled to a two-temperature model [33], to assess whether the above assumptions are consistent with the main features of our observations, providing an insight into the underlying reversal process taking place at the picosecond time scale.

The model accounts for two key features: (i) the rapid drop of the uniaxial anisotropy K_u with temperature and (ii) the small tilt of the uniaxial anisotropy axis with respect to the out-of-plane direction, chosen to be toward the x axis, $\mathbf{u_k} = (\sin\theta_u, 0, \cos\theta_u)$, $\theta_u > 0°$. The energy density of the system, assuming a continuous-film approximation, is given by $E_{\text{tot}} = -K_u(\mathbf{u_k} \cdot \mathbf{m})^2 + \frac{1}{2}\mu_0 M_S^2 m_z^2$, where $\mathbf{m}$ is the unitary vector. The phenomenological relation used for the anisotropy is $K_u(T) = K_{u0}[1 - (T/T_C)^{1.73}]^2$, where $T_C = 450$ K is a critical temperature [34]. As a first approximation, the simulations were performed assuming constant M_s and, as a consequence, constant demagnetizing anisotropy $K_d = \frac{1}{2}\mu_0 M_s^2$. The fact that in the Co-rich region, M_s is expected to increase with the temperature [21] is not a concern, as this would further promote the in-plane reorientation. This instead is not true for the Tb-rich region, where M_s is expected to drop rapidly with the temperature and no AOS is observed.

In Fig. 2(d), the calculation for the reversal mechanism is shown for $\theta_u = 5°$ at increasing fluence (columns 2, 3, and 4) and compared with column 1, where no tilt is present. After the laser pulse, the demagnetizing field overcomes the anisotropy and the magnetization starts precessing toward the plane. If $\theta_u = 0°$, the precession occurs only around the z axis and no crossing of the x-y plane is possible. Instead, the small tilt introduces a x component in the effective field [$\mathbf{H}_{\text{eff}} = -(1/\mu_0 M_s)(\delta E_{\text{tot}}/\delta\mathbf{m})$] that strongly affects the trajectory of the magnetization and drives the reversal.

The precession occurs for a time that depends on the energy absorbed, i.e., the laser fluence. The anisotropy field recovers during the precession due to cooling ($K_d < K_u$). As the fluence increases, the number of rotations made by the magnetization during precession increases. Depending on whether the number of half rotations is odd or even, the magnetization will end up as reversed or not reversed, resulting in the pattern of concentric rings shown in Figs. 1(c), 2(b), and 2(c).

Although the model is fairly simple, it is able to correctly predict the main features of our [Tb/Co] multilayer system. The perpendicular anisotropy originating from the Tb-Co interface [35] is known to have an important temperature dependence, with typical blocking temperatures below 200 °C due to the low Curie temperature of Tb (237 K for bulk measurements [36]). The assumption of a tilted axis for the anisotropy is supported by the quasistatic measured hysteresis loop in Fig. 4(c), showing a gradual saturation for higher perpendicular fields, which indicates the existence of an in-plane component. The presence of in-plane uniaxial anisotropy in [Tb/Co] multilayers has already been reported [35], providing further justification for considering it. The origin of a local tilt may be attributed to the sperimagnetic nature of Tb [37] or the polycrystalline nature of the Tb/Co multilayer. According to our simulation, to have magnetization reversal, the

perfect out-of-plane symmetry has to be broken and thus the tilt angle needs to be greater than 0°. We have observed that lower the tilt angle, the smaller is the fluence switching window. We have chosen a value of 5°, as the fluence required to commute was consistent with the experimental observations. Our additional simulations indicate that equivalent behavior is found for a tilt angle between 2 and 15°. The fluence threshold would change with the tilt value in this window but the overall behavior is similar. As shown by the magnetization time traces in Fig. 2(d), the total time for reversal is expected to be of the order of tens to hundreds of picoseconds but the final magnetization state is determined by the first few precessions. Currently, our model presents one possible scenario, to be confirmed by future work. It offers a strong and coherent grasp of the observed magnetization-reversal behaviors, even without factoring in the rapid partial demagnetization caused by the sudden rise in electron temperature. Addressing this requires more detailed atomistic or Landau-Lifshitz-Bloch (LLB) models, which we plan to explore in an upcoming study.

Next, we have introduced the Tb/Co-based thin films as storage layers in full MTJ stacks with optical access, enabling AOS writing and electrical readout. Nanopillars have been fabricated on a cross-wedge thickness sample annealed at 250 °C, keeping the Co-layer thickness fixed at 1.4 nm while varying the Tb-layer thickness from 0.4 nm to 1.1 nm across a 100-mm Si(100) wafer, to include the known AOS thickness region for Tb of 0.7–0.9 nm. Perpendicularly, a cross wedge of the MgO barrier has been deposited, with a thickness ranging from 1.1 to 3.0 nm, to characterize the optimal Mg natural-oxidation thickness to achieve the highest TMR ratio.

The nanofabrication process includes indium tin oxide (ITO) as a transparent conductive electrode to provide optical access to the top electrode of the MTJ (for details, see Ref. [38]). Fabricated MTJ devices with diameters from 300 nm down to 80 nm show no impact on the expected AOS stack properties from the reference layer, with typical offset fields below 200 Oe. Indeed, high perpendicular anisotropy at the film level is maintained after nanopatterning, as shown by the patterned and thin-film coercivity in Fig. 3(b). The coercivity depends on the Tb/Co thickness but stays comparable before and after patterning, without any substantial dependence on the diameter. The device-average TMR values for each pillar, of nominal diameter ranging from 80 to 300 nm, versus the naturally oxidized MgO thickness are compared with the literature values in Fig. 3(a), for a Tb thickness of 0.5 nm. The natural oxidation time was fixed to two steps of 10 s at 150 mbar. The optimal Mg thickness is 2 nm: below this value, the tunnel barrier is overoxidized, leading to lower TMR values. This stable reference layer combined with the optimized Mg natural-oxidation thickness allows us to obtain highest TMR values of 74%, representing a
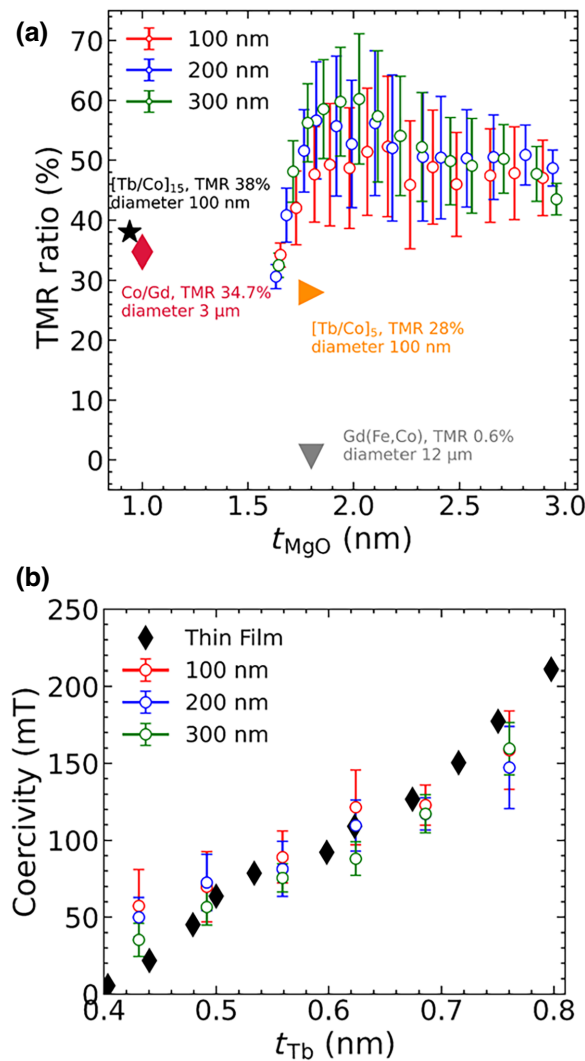
FIG. 3.   (a) The device-average TMR versus the naturally oxidized MgO thickness for a nominal diameter between 100 and 300 nm and thicknesses t_{Tb} ranging from 0.5 nm to 0.75 nm and $t_{Co} = 1.4$ nm, respectively, compared with the literature values [20,24,25,38]. (b) A comparison of the coercive field versus the Tb thickness between a thin-film sample and nanopatterned devices.
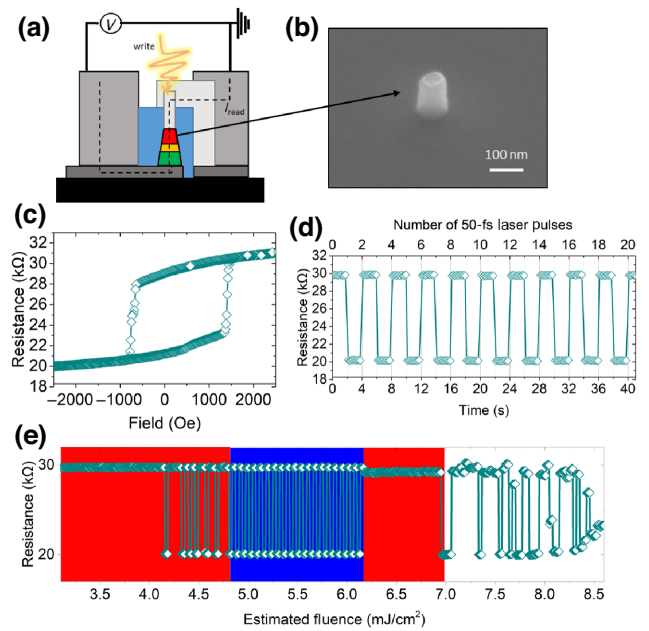

FIG. 4.   (a) A schematic illustration of the all-optical writing and electrical reading of an AOS MTJ. (b) An SEM image of a 100-nm diameter pillar. (c) An AOS-MTJ hysteresis *R-H* loop, with the field applied out of plane. (d) A TMR measurement as a function of the time upon laser-pulse excitation. (e) A TMR measurement using a constant 1-Hz laser frequency and incremental laser power for each pulse.

factor-of-2 improvement compared with the highest AOS MTJ reported so far [19,20,24,25,38].

The all-optical switching properties of the nanosize MTJ pillars were investigated using linearly polarized femtosecond laser pulses while measuring the resistance of the junction, as illustrated in the schematics of Fig. 4(a). The electrical readout was performed using a digital multimeter connected to the device top and bottom electrodes by wire bonding. The resistance was measured by applying a continuous reading voltage of 10 mV. All measurements were performed without any external magnetic field, without compensating offset fields from the reference layer. Figure 4(d) shows an example of a 100-nm AOS MTJ that

can be repeatedly toggled between parallel (P) and antiparallel (AP) states, showing the full 50% TMR resistance change expected from the *R-H* loop in Fig. 4(c).

The absorbed energy, calculated assuming a 17.5% absorption of the laser fluence (from Ref. [39] on a similar stack) multiplied by the area of the pillar, was estimated to be 68.6 fJ/bit. This is already much lower than the dissipation writing energy of existing technologies such as hard-disk drives (10–100 nJ) [40], flash memory (10 nJ) [41], and state-of-the-art STT-RAM (450 pJ to 100 fJ) [3,42] but the corresponding energy for a pillar of diameter 40 nm is 11 fJ/bit, 45% less than the prediction in Ref. [3].

In Fig. 4(e), we compare the fluence write levels between the patterned tunnel junction and the equivalent AOS stack at thin-film level. The switching dependence on the fluence appears to be preserved after patterning. In the performed experiment, the laser was shot repeatedly at a frequency of 1 Hz, while increasing the laser power with a step of 0.01 mW every second. This allows us to probe the minimum fluence for which a reversal is obtained. At low fluence, there is no switching; some switching events are observed starting at 4 mJ/cm^2. In the region of 5–6 mJ/cm^2, the switching probability is 100%, as highlighted in blue in Fig. 4. For even higher fluence, in the region highlighted in red, switching is no longer observed, followed by random switching before an eventual device degradation. There is a strong correlation

between this established device phase diagram and that of the thin film from Fig. 1(d), indicative of a very similar reversal mechanism responsible for the alternating of the reversal and nonreversal regions. In the framework of our model, the same precessional switching-reversal process determines the AOS properties of the patterned device, despite the fact that some stray field from the reference layer is acting on the storage layer.

III. CONCLUSIONS

In conclusion, we have integrated a bottom-reference p-MTJ with an all-optical-switchable $[Tb/Co]_{\times 5}$-based storage layer, the resulting continuous film and patterned devices having similar magnetic properties. This system shows all-optical-switching for Co-rich regions close to the magnetization compensation region at room temperature for a Tb thickness range of 0.6–0.9 nm, and for a Co thickness range of 1.2–1.5 nm. We have developed a macrospin model able to predict several of the characteristic features that are observed experimentally. Thus the magnetization-reversal process appears to be driven by an in-plane reorientation of the magnetization coupled to a precessional switching mechanism. The model explains the experimentally observed concentric rings of opposite magnetization directions that appear at high laser fluence. Remarkably, both the experiments and the simulations indicate that the threshold fluences do not depend on the pulse duration but, rather, on the AOS layer thicknesses. This represents a significant advantage of the Tb/Co material, which provides high resilience to pulse-length variability at the device level. Furthermore, the implementation of a stable reference layer and optimization of the MgO natural oxidation has allowed for TMR values of 74%, the highest reported so far for AOS MTJs. Field-free helicity-independent all-optical toggle switching has been demonstrated on 100-nm patterned [Tb/Co] p-MTJ devices, driven by 50-fs laser pulses for an absorbed energy of 68.6 fJ/bit. These findings hopefully pave the way toward nanoscale devices for optospintronic embedded memories combining nonvolatility with ultrafast and energy-efficient writing.

[1] B. Dieny, I. L. Prejbeanu, K. Garello, P. Gambardella, P. Freitas, R. Lehndorff, W. Raberg, U. Ebels, S. O. Demokritov, and J. Akerman, *et al.*, Opportunities and challenges for spintronics in the microelectronics industry, Nat. Electron. **3,** 446 (2020).

[2] J. Kim, A. Paul, P. A. Crowell, S. J. Koester, S. S. Sapatnekar, J.-P. Wang, and C. H. Kim, Spin-based computing: Device concepts, current status, and a case study on a high-performance microprocessor, Proc. IEEE **103,** 106 (2014).

[3] A. V. Kimel and M. Li, Writing magnetic memory with ultrashort light pulses, Nat. Rev. Mater. **4,** 189 (2019).

[4] J. C. Slonczewski, Current-driven excitation of magnetic multilayers, J. Magn. Magn. Mater. **159,** L1 (1996).

[5] L. Berger, Emission of spin waves by a magnetic multilayer traversed by a current, Phys. Rev. B **54,** 9353 (1996).

[6] D. C. Ralph and M. D. Stiles, Spin transfer torques, J. Magn. Magn. Mater. **320,** 1190 (2008).

[7] S. Yuasa, T. Nagahama, A. Fukushima, Y. Suzuki, and K. Ando, Giant room-temperature magnetoresistance in single-crystal Fe/MgO/Fe magnetic tunnel junctions, Nat. Mater. **3,** 868 (2004).

[8] S. S. Parkin, C. Kaiser, A. Panchula, P. M. Rice, B. Hughes, M. Samant, and S.-H. Yang, Giant tunnelling magnetoresistance at room temperature with MgO (100) tunnel barriers, Nat. Mater. **3,** 862 (2004).

[9] A. Brataas, A. D. Kent, and H. Ohno, Current-induced torques in magnetic materials, Nat. Mater. **11,** 372 (2012).

[10] K. Ando, S. Fujita, J. Ito, S. Yuasa, Y. Suzuki, Y. Nakatani, T. Miyazaki, and H. Yoda, Spin-transfer torque magnetoresistive random-access memory technologies for normally off computing, J. Appl. Phys. **115,** 172607 (2014).

[11] A. Khvalkovskiy, D. Apalkov, S. Watts, R. Chepulskii, R. Beach, A. Ong, X. Tang, A. Driskill-Smith, W. Butler, and P. Visscher, *et al.*, Basic principles of STT-MRAM cell operation in memory arrays, J. Phys. D: Appl. Phys. **46,** 074001 (2013).

[12] A. Manchon, J. Železný, I. M. Miron, T. Jungwirth, J. Sinova, A. Thiaville, K. Garello, and P. Gambardella, Current-induced spin-orbit torques in ferromagnetic and antiferromagnetic systems, Rev. Mod. Phys. **91,** 035004 (2019).

[13] I. M. Miron, K. Garello, G. Gaudin, P.-J. Zermatten, M. V. Costache, S. Auffret, S. Bandiera, B. Rodmacq, A. Schuhl, and P. Gambardella, Perpendicular switching of a single ferromagnetic layer induced by in-plane current injection, Nature **476,** 189 (2011).

[14] V. Krizakova, M. Perumkunnil, S. Couet, P. Gambardella, and K. Garello, Spin-orbit torque switching of magnetic tunnel junctions for memory applications, J. Magn. Magn. Mater. **562,** 169692 (2022).

[15] C. D. Stanciu, F. Hansteen, A. V. Kimel, A. Kirilyuk, A. Tsukamoto, A. Itoh, and T. Rasing, All-Optical Magnetic Recording with Circularly Polarized Light, Phys. Rev. Lett. **99,** 047601 (2007).

[16] I. Radu, K. Vahaplar, C. Stamm, T. Kachel, N. Pontius, H. Dürr, T. Ostler, J. Barker, R. Evans, and R. Chantrell, *et al.*, Transient ferromagnetic-like state mediating ultrafast reversal of antiferromagnetically coupled spins, Nature **472,** 205 (2011).

[17] T. Ostler, J. Barker, R. Evans, R. Chantrell, U. Atxitia, O. Chubykalo-Fesenko, S. El Moussaoui, L. Le Guyader, E. Mengotti, and L. Heyderman, *et al.*, Ultrafast heating as a sufficient stimulus for magnetization reversal in a ferrimagnet, Nat. Commun. **3,** 666 (2012).

[18] E. Y. Vedmedenko, R. K. Kawakami, D. D. Sheka, P. Gambardella, A. Kirilyuk, A. Hirohata, C. Binek, O. Chubykalo-Fesenko, S. Sanvito, and B. J. Kirby, *et al.*, The 2020 magnetism roadmap, J. Phys. D: Appl. Phys. **53,** 453001 (2020).

[19] L. Avilés-Félix, L. Álvaro-Gómez, G. Li, C. Davies, A. Olivier, M. Rubio-Roy, S. Auffret, A. Kirilyuk, A. Kimel, and T. Rasing, *et al.*, Integration of tb/co multilayers within optically switchable perpendicular magnetic tunnel junctions, AIP Adv. **9,** 125328 (2019).

[20] L. Avilés-Félix, A. Olivier, G. Li, C. S. Davies, L. Álvaro-Gómez, M. Rubio-Roy, S. Auffret, A. Kirilyuk, A. Kimel, and T. Rasing, *et al.*, Single-shot all-optical switching of magnetization in Tb/Co multilayer-based electrodes, Sci. Rep. **10,** 5211 (2020).

[21] K. Mishra, T. G. H. Blank, C. S. Davies, L. Avilés-Félix, D. Salomoni, L. D. Buda-Prejbeanu, R. C. Sousa, I. L. Prejbeanu, B. Koopmans, T. Rasing, A. V. Kimel, and A. Kirilyuk, Dynamics of all-optical single-shot switching of magnetization in Tb/Co multilayers, Phys. Rev. Res. **5,** 023163 (2023).

[22] Y. Peng, D. Salomoni, G. Malinowski, W. Zhang, J. Hohlfeld, L. D. Buda-Prejbeanu, J. Gorchon, M. Vergès, J. X. Lin, D. Lacour, *et al.*, In-plane reorientation induced single laser pulse magnetization reversal, Nat. Commun. **14,** 5000 (2023).

[23] J. Igarashi, W. Zhang, Q. Remy, E. Díaz, J.-X. Lin, J. Hohlfeld, M. Hehn, S. Mangin, J. Gorchon, and G. Malinowski, Optically induced ultrafast magnetization switching in ferromagnetic spin valves, Nat. Mater. **22,** 725 (2023).

[24] J.-Y. Chen, L. He, J.-P. Wang, and M. Li, All-Optical Switching of Magnetic Tunnel Junctions with Single Subpicosecond Laser Pulses, Phys. Rev. Appl. **7,** 021001 (2017).

[25] L. Wang, H. Cheng, P. Li, Y. L. van Hees, Y. Liu, K. Cao, R. Lavrijsen, X. Lin, B. Koopmans, and W. Zhao, Picosecond optospintronic tunnel junctions, Proc. Natl. Acad. Sci. **119,** e2204732119 (2022).

[26] S. Mondal, D. Polley, A. Pattabi, J. Chatterjee, D. Salomoni, L. Aviles-Felix, A. Olivier, M. Rubio-Roy, B. Diény, L. D. B. Prejbeanu, R. Sousa, I. L. Prejbeanu, and J. Bokor, Single-shot switching in Tb/Co-multilayer based nanoscale magnetic tunnel junctions, J. Magn. Magn. Mater. **581,** 170960 (2023).

[27] F. Dumas-Bouchiat, H. Nagaraja, F. Rossignol, C. Champeaux, G. Trolliard, A. Catherinot, and D. Givord, Cobalt cluster-assembled thin films deposited by low energy cluster beam deposition: Structural and magnetic investigations of deposited layers, J. Appl. Phys. **100,** 064304 (2006).

[28] F. Darnell, Lattice parameters of terbium and erbium at low temperatures, Phys. Rev. **132,** 1098 (1963).

[29] J. Yue, S. Jiang, D. Zhang, H. Yuan, Y. Wang, L. Lin, Y. Zhai, J. Du, and H. Zhai, The influence of interface on spin pumping effect in $Ni_{80}Fe_{20}$/Tb bilayer, AIP Adv. **6,** 056120 (2016).

[30] A. Rebei and J. Hohlfeld, Origin of Increase of Damping in Transition Metals with Rare-Earth-Metal Impurities, Phys. Rev. Lett. **97,** 117601 (2006).

[31] G.-M. Choi, B.-C. Min, K.-J. Lee, and D. G. Cahill, Spin current generated by thermally driven ultrafast demagnetization, Nat. Commun. **5,** 4334 (2014).

[32] E. Beaurepaire, J.-C. Merle, A. Daunois, and J.-Y. Bigot, Ultrafast Spin Dynamics in Ferromagnetic Nickel, Phys. Rev. Lett. **76,** 4250 (1996).

[33] L. Avilés-Félix, L. Farcis, Z. Jin, L. Álvaro-Gómez, G. Li, K. T. Yamada, A. Kirilyuk, A. V. Kimel, T. Rasing, and B. Dieny, *et al.*, All-optical spin switching probability in [Tb/Co] multilayers, Sci. Rep. **11,** 6576 (2021).

[34] D. S. Hazen, S. Auffret, I. Joumard, L. Vila, L. D. Buda-Prejbeanu, R. C. Sousa, L. Prejbeanu, and B. Dieny, Double magnetic tunnel junctions with a switchable assistance layer for improved spin transfer torque magnetic memory performance, Nanoscale **13,** 14096 (2021).

[35] L. Ertl, G. Endl, and H. Hoffmann, Structure and magnetic properties of sputtered Tb/Co multilayers, J. Magn. Magn. Mater. **113,** 227 (1992).

[36] W. Thoburn, S. Legvold, and F. Spedding, Magnetic properties of terbium metal, Phys. Rev. **112,** 56 (1958).

[37] J. Coey, Amorphous magnetic order, J. Appl. Phys. **49,** 1646 (1978).

[38] A. Olivier, L. Avilés-Félix, A. Chavent, L. Álvaro-Goémez, M. Rubio-Roy, S. Auffret, L. Vila, B. Dieny, R. C. Sousa, and I. Prejbeanu, Indium tin oxide optical access for magnetic tunnel junctions in hybrid spintronic-photonic circuits, Nanotechnology **31,** 425302 (2020).

[39] E. K. Sobolewska, J. Pelloux-Prayer, H. Becker, G. Li, C. S. Davies, C. Krückel, L. A. Félix, A. Olivier, R. C. Sousa, and I.-L. Prejbeanu, *et al.*, in *Active Photonic Platforms XII*, Vol. 11461 (SPIE, 2020), p. 54.

[40] A. Hylick, R. Sohan, A. Rice, and B. Jones, in 2008 IEEE International Symposium on Modeling, Analysis and Simulation of Computers and Telecommunication Systems (IEEE, 2008), p. 1.

[41] J. P. Liu, E. Fullerton, O. Gutfleisch, and D. J. Sellmyer, *Nanoscale Magnetic Materials and Applications* (Springer, 2009).

[42] K. Wang, J. Alzate, and P. K. Amiri, Low-power non-volatile spintronic memory: STT-RAM and beyond, J. Phys. D: Appl. Phys. **46,** 074003 (2013).